Using Cell Cycle Measurements with Flow Cytometry to Predict the Growth Rate of Walleye Pollock *Gadus chalcogrammus* Larvae

Steven M. Porter[1*] and Annette B. Dougherty[1]

[1*]Corresponding author. Recruitment Processes Program, Resource Assessment and Conservation Engineering Division, Alaska Fisheries Science Center, NOAA, National Marine Fisheries Service, 7600 Sand Point Way NE, Seattle, Washington 98115, USA
E-mail address: steve.porter@noaa.gov (S.M. Porter)

Published in the Journal of Experimental Marine Biology and Ecology 2019
https://doi.org/10.1016/j.jembe.2019.151178

Abstract

Growth rate during early life stages can be an important factor in the recruitment process of marine fishes, and in this study we develop a methodology based on cell cycle measurements to predict the growth rate of Walleye Pollock (*Gadus chalcogrammus*) larvae. Results from cell-cycle analysis of muscle cell nuclei of laboratory-reared Walleye Pollock larvae measured with flow cytometry were used as covariates in a generalized additive model to predict the growth rate (growth in length per day, mm d^{-1}) of individual larvae from the day exogenous feeding began (first feeding) to the time of capture ($r^2 = 0.79$). Additional covariates used were temperature and standard length. A generalized additive model to classify a larva as fast- or slow-growing was also formulated using the same covariates. Validation testing with an independent set of 45 laboratory-reared larvae showed that 33% of the laboratory growth rates (i.e., growth rate based on age and size) fell within the 95% confidence interval of the predicted growth rates, and predicted growth rates were significantly less than otolith-derived growth rates. The growth classification model was more accurate than the growth rate model, correctly classifying the growth rate type (fast or slow growing) of 71% of the same set of larvae showing that flow cytometric cell cycle analysis may be better suited for classifying larvae as fast- or slow-growing rather than for predicting absolute growth rate. Predicted growth rates for larvae ≤ 11 mm in length collected from the Gulf of Alaska were within the range of published values for that area, and were not significantly different than corresponding otolith-derived growth rates. The growth rates of Gulf of Alaska larvae > 11 mm were overestimated when compared to both otolith-derived growth rates and published values, and that may be due in part because those larvae were outside of the size range used to formulate the model. Predicted growth rate and growth classification of late-stage, field-collected Walleye Pollock larvae would be improved by

adding larvae as large as 15 mm to the model to encompass the size range of larvae typically collected during spring ichthyoplankton surveys conducted in the Bering Sea or Gulf of Alaska. Flow cytometric cell cycle analysis offers promise as an alternative method for determining growth rate of fish larvae when otolith daily increments cannot be reliably counted.

Keywords

Flow cytometry

Cell cycle

Growth rate

Fish larvae

Walleye Pollock

Gadus chalcogrammus

Introduction

Growth rate plays a crucial role in determining survival during the larval stage of marine fishes, and small changes in growth or mortality rates during early life may affect year-class strength (Houde, 1987). The 'growth-mortality' hypothesis is used to explain survival of marine fish larvae and is based on fast growth being advantageous (Anderson, 1988). Components of that hypothesis are the 'bigger is better', 'growth rate', and 'stage duration' hypotheses. The 'bigger is better' hypothesis states that for individuals of the same age, larger larvae are more likely to survive than smaller ones due to size-dependent predation mortality (Leggett and DeBlois, 1994). A decrease in the growth rate of fish larvae due to suboptimal prey abundance or temperature or other unfavorable environmental conditions can increase the duration that high mortality rates operate over (Houde, 1987). The 'growth rate' hypothesis relates fast growth to reducing the amount of time spent at sizes where mortality rates are highest (Ware, 1975). The 'stage duration' hypothesis is based on fast growth reducing the amount of time an individual spends in the high mortality larval stage; that is, increased survival by transitioning to the juvenile stage sooner (Chambers and Leggett, 1987). Thus, an individual's survival is affected by both its growth rate and size-specific mortality rate. Model simulations have shown selectivity for fast-growing larvae (Rice et al., 1993; Akimova et al., 2016). For example, 80% of Bloater *Coregonus hoyi* larvae surviving to day 60 came from the upper 25% of the initial growth rate distribution (Rice et al., 1993), most likely because of reduced mortality with increasing size. Atlantic Cod *Gadus morhua* larvae surviving through settlement in the North Sea had growth rates approximately equal to fish fed *ad libitum* in the laboratory (Akimova et al., 2016). Field studies also show selection for faster growing fish larvae. Slow-growing Japanese Anchovy *Engraulis japonicus* larvae were more likely to be preyed upon than faster growing individuals

(Takasuka et al., 2003, 2004). Otolith microstructure analysis showed that fast-growing Atlantic Cod larvae, and Bluefish *Pomatomus saltatrix* larvae had higher survival (Meekan and Fortier, 1996; Hare and Cowen, 1997). Walleye Pollock larvae in the Bering Sea grew faster and had higher survival into summer during relatively warm years compared to cold years (Hunt et al., 2011). A laboratory study of yellowtail kingfish, *Seriola lalandi*, larvae reared under projected climate change conditions (increasing ocean temperature and pCO_2) showed that larvae at 25°C grew and morphologically developed faster than larvae at 21°C, but larvae at the higher temperature had lower survival (Watson et al., 2018) indicating that future climate change could negate the advantage of growing fast because of higher mortality. Growth during the larval stage may also affect over-winter survival of young-of-the-year, larger young-of-the-year Walleye Pollock *Gadus chalcogrammus* are more likely to survive than smaller individuals (Heintz and Vollenweider, 2010).

Otolith microstructure analysis, the RNA-DNA ratio, and flow cytometric cell-cycle analysis have been used to estimate growth rates of fish larvae (Dougherty, 2008; Caldarone et al., 2003; Caldarone, 2005; Theilacker and Shen, 2001; Domingos et al., 2012). The number of otolith increments and/or increment width is widely used to estimate the growth rate of fish larvae and typically involves counting the daily increments formed on the otolith and then modeling growth based on size at age (Dougherty, 2008). Problems with that method arise from increment compression due such conditions as cold temperature or lack of prey that slow growth and hamper the ability to reliably age larvae. The RNA-DNA ratio and temperature have been used to model protein-specific, short-term growth rate of Atlantic Cod and Haddock *Melanogrammus aeglefinus* larvae (Caldarone et al., 2003; Caldarone, 2005), and weight-specific growth rate for different species of fish larvae (Buckley et al., 2008). The amount of variance in growth rate

explained by those models ranged from 39% to 82%. Using flow cytometric cell-cycle analysis to estimate larval growth is based on the premise that cell proliferation is related to somatic growth rate. In flow cytometry, individual cells or nuclei are stained with target-specific dyes, passed through laser beams, and their fluorescence is measured. Flow cytometric cell-cycle analysis is a technique that measures the DNA content of individual cells in a population based on their fluorescence to determine the proportion of cells in different stages of the cell cycle, and can be used on specific tissues of individual fish larvae or whole larva homogenates (Theilacker and Shen, 2001; Domingos et al., 2012). The cell cycle is divided into two parts: interphase and mitosis (M). Interphase consists of three stages: gap 1 (G1), DNA synthesis (S), and gap 2 (G2). Cell growth occurs during the G1 stage before cell division begins, and cells may enter a G0 resting state after this phase in response to starvation or other unfavorable environmental conditions (Murray and Hunt, 1993). For cells to divide they must first replicate their DNA (S), and then grow and produce the structures necessary for mitosis (G2). The DNA content of cells in the S-stage increases to up to twice the amount of DNA as G1 stage cells. G2 and mitosis (before cell division) stage cells have twice the amount of DNA as G1 stage cells. The fraction of cells in S, and G2 and mitosis (hereafter referred to as G2 and M) are indicative of cells that may divide. For Walleye Pollock larvae the fraction of cells in S, and G2 and M-stages are responsive to recent feeding history (Theilacker and Shen, 2001; Porter and Bailey, 2011) and can indicate changes in cell division. The fraction of S-stage nuclei of muscle cells of Walleye Pollock larvae significantly decreased after a few days of prey being withheld ($\leq$ 3d, Porter and Bailey, 2011) suggesting reduced cell division. The fraction of G2 and M-stage nuclei increased during starvation (Porter and Bailey, 2011) and may indicate cells staying in the G2-stage due to a checkpoint between this stage and mitosis that slows or halts cell division if energy reserves are

low (Murray and Hunt, 1993). Cell-cycle analysis of muscle tissue of Walleye Pollock larvae (Theilacker and Shen, 2001), and whole Barramundi *Lates calcarifer* larvae (Domingos et al., 2012) has shown that the fraction of cells dividing (S + G2 and M stages) is positively correlated with both larval size and growth in length. For both studies slightly more than 50% of the variance was explained in models using cell cycle analysis to estimate growth of those larvae (Theilacker and Shen, 2001; Domingos et al., 2012).

Measuring the growth rate of marine fish larvae is valuable for understanding recruitment dynamics because fast growth increases the probability of surviving this life stage. In this study we formulate and test a generalized additive model to predict the growth rate (growth in length per day, mm d^{-1}) of individual Walleye Pollock larvae using covariates from cell-cycle analysis with flow cytometry, temperature, and standard length. This approach may offer an alternative for growth rate estimates when otolith microstructure analysis is unreliable. The model was developed and validated with laboratory-reared larvae and then tested on larvae collected from the Gulf of Alaska. Growth rates predicted from the model and those calculated from otolith microstructure analysis were compared.

Material and methods

1.1 Laboratory rearing and growth studies

Adult Walleye Pollock were collected by trawl in Shelikof Strait, Gulf of Alaska, during the spawning season in March 2014, 2015, and 2017. Eggs from single fish pairings (one female and one male) were fertilized and maintained aboard ship in the dark at 3°C before being transported to the Alaska Fisheries Science Center, Seattle, WA. Larvae were reared at 3.2º and 6.1ºC in 2014, 1.6º and 3.0ºC in 2015, and 8.3ºC in 2017 (Table 1). All rearing experiments used one-

142 micron filtered seawater (33 PSU) and a 16-hour daylight cycle with a 2.5 μmol photon m^{-2} s^{-1}
143 light level at the water surface from overhead full spectrum fluorescent lights. Two replicate 20
144 L black, circular tanks each containing approximately 500 larvae were used for each temperature
145 and feeding treatment following procedures described in Porter and Theilacker, 1996. Feeding
146 treatments for the 3.2º, 6.1º, and 8.3ºC experiments were high density of prey (10 rotifer ml^{-1} and
147 3 natural zooplankton ml^{-1}), low prey density (1.0 natural zooplankton ml^{-1}), and an unfed
148 treatment (Table 1). Natural zooplankton, which included primarily copepod nauplii (*Acartia*
149 spp.) and gastropod veligers, were collected from a local lagoon and screened through a 202-μm
150 mesh. The high prey density treatment at 1.6ºC did not use rotifer prey because they become
151 inactive and settle out of the water column at that temperature. Instead a zooplankton density of
152 10 ml^{-1} was used and the other treatments remained unchanged. Removing the rotifers and
153 increasing the density of zooplankton to 10 ml^{-1} should not negatively affect larval growth rate
154 because Walleye Pollock larvae fed natural zooplankton grow faster than those fed rotifers
155 (Porter and Bailey, 2007). Thus the growth rate of larvae fed 10 ml^{-1} zooplankton would be
156 expected to be at least equal to that of larvae fed the high density rotifer and zooplankton diet.
157 First feeding was defined as the first day when 50% of the larvae were observed feeding. Mean
158 standard length (SL) of 10 larvae at first feeding for each feeding treatment and temperature
159 were used as the size at that stage when calculating laboratory growth rate. Here laboratory
160 growth rate is defined as growth beginning at first feeding determined from known age and size
161 in the laboratory. For each larva from a specific feeding treatment and temperature, laboratory
162 growth rate was calculated as the difference between size at capture and mean SL at first feeding,
163 divided by the number of days after first feeding. Treatments were sampled three or four times at
164 intervals based on equivalent degree-days among rearing temperatures, ranging from 3 to 12

days between sampling depending on temperature. Larvae in the 1.6ºC treatment were sampled on the same days as the 3ºC treatments. This ensured that an adequate sample number was taken due to high mortality that was expected to occur at this temperature. The 2015 experiment was designed to take into account the effect of intermittent feeding on growth. This experiment was conducted at 3.0ºC using larvae starved for 6 days after first feeding and then fed at the high prey density treatment, and another treatment that fed at high prey density for 6 days after first feeding followed by starvation. An always-fed high prey density treatment was used as a control. For all experiments the number of larvae taken from a tank on a given sampling day ranged from 5 to 36 depending on whether larvae would also be used for model validation testing. Larvae taken from rearing tanks were euthanized in a 1% solution of tricaine methanesulfonate (MS-222), and then a digital photograph was taken of each larva before it was frozen at -80°C. Calibrated digital photographs were used to measure SL and body depth at anus (BDA) of each larva using Image-Pro Plus vers. 4.5 (Media Cybernetics, Inc., Rockville, MD) image analysis software.

1.2 Flow cytometry

DAPI (4',6-diamidino-2-phenylindole), a fluorescent DNA stain, was used at a concentration of 10 μg mL^{-1} for cell-cycle analysis with flow cytometry. Nuclear RNA was stained with Invitrogen Syto RNASelect green fluorescent cell stain (S32703, Life Technologies Corp., Carlsbad, CA; hereafter referred to as Syto RNASelect stain) and was used at a concentration of 1000 nM. Tissue preparation, DNA and RNA staining protocols followed Porter and Bailey (2011 and 2013), modified from Theilacker and Shen (2001). A frozen larva was placed into an approximately 100 μL mixture of DAPI and Syto RNASelect stains on a glass depression slide. The head and gut were dissected away from the trunk musculature, and the tissue was sliced into

4–5 pieces with 2 scalpels. The pieces of the trunk musculature were transferred into a microcentrifuge tube that contained a 230-µL mixture of DAPI and Syto RNASelect stains and then the mixture was triturated 6 times using a 1mL syringe with a 25-gauge needle to release the nuclei from the cells. The solution was filtered through a 48-µm filter into another microcentrifuge tube to separate the stained nuclei from large cellular debris. Prepared samples were kept on ice until they were analyzed with a BD Biosciences LSRII flow cytometer (BD Biosciences, San Jose, CA), typically within 6 hours of preparation. DAPI was excited with a 405 nm, 100 mW violet laser, and Syto RNASelect stain was excited with a 488 nm, 100 mW blue laser. The DAPI/DNA detector filter was 450/50, and filters used for Syto RNASelect stain/RNA were 505 long pass and 530/30.

Chicken erythrocyte nuclei (Biosure, Inc., Grass Valley, CA) stained with the same mixture of DAPI and Syto RNASelect dyes were used as flow cytometry controls. At the beginning of each flow cytometry session, the control was run and necessary adjustments were made to the laser voltages to keep control fluorescence values similar to previous sessions. Cell cycle analysis is sensitive to tissue quality. High-quality tissue preparation (i.e., quickly freezing larvae and minimizing tissue processing time) is necessary to keep the amount of tissue debris in prepared samples low, and this in turn results in small coefficients of variation for G0 and G1. Samples that had < 5000 nuclei analyzed or a coefficient of variation for G0 and G1 > 9.00 were not used in further analyses and this criteria resulted in rejection of about a third of all samples.

For each larva, the fraction of nuclei in G0 and G1, S, and G2 and M stages of the cell cycle were calculated using MultiCycle AV software, vers. 4.0 (Phoenix Flow Systems, San Diego). FCS Express flow cytometry analysis software, vers. 3.0 (De Novo Software, Los Angeles) was used to calculate the ratio of the number of S-stage nuclei to the number of G1-

stage nuclei with high RNA content (Porter and Bailey 2013; hereafter, this ratio will be referred to as RSG1). RSG1 is a measure of potential cell division based on progression of nuclei from the G1 to S stage. Slower growing larvae may have fewer dividing cells and thus potentially less S-stage nuclei, so the ratio of S to G1 nuclei may vary with growth rate (Porter and Bailey, 2013).

1.3 Otolith microstructure analysis

Heads from frozen larvae were preserved in 100% ethanol after thawing. Otoliths were prepared for microstructure analysis as described in Dougherty (2008). For each larva, otoliths were dissected from the head and mounted to glass microscope slides using clear acrylic finger nail polish. Walleye Pollock larvae deposit increments on their otoliths daily (Dougherty, 2008) and their otoliths typically have an optically distinct increment representing the day of first feeding (Bailey and Stehr, 1988). Otolith increment width is a relative measure of somatic growth between days that the increments were deposited (Campana, 1996). Increments from first-feeding to the otolith edge of both sagitta otoliths were counted, and that distance was measured to nearest micron with an ocular micrometer at 1000X magnification using a compound microscope. Both measurements correspond with growth from first feeding to capture. Otoliths were read and measured along the maximum diameter axis, and the largest value for increment number and distance was recorded.

1.4 Growth model formulation and validation

Generalized additive models (GAM; Wood, 2006) were used to predict the growth rate (growth in length per day, mm d^{-1}) of a larva from the start of exogenous feeding (first feeding) to the time of capture. GAMs are non-parametric regression techniques, in which the effect of a covariate is estimated with a smooth function, typically a natural cubic spline, and therefore may

not necessarily be linear (Wood, 2006). Beginning at first feeding, larvae are dependent upon their surrounding environment for energy, and measuring growth during at this stage gives an overall indication of how well a larva has been feeding and growing. Laboratory growth rate was used as the response variable, and the independent variables (covariates) were SL, BDA, temperature, fraction of S-stage nuclei, fraction of G2-and-M-stage nuclei, and RSG1. The arcsin $\sqrt{x}$ transformation was used to normalize the fraction of S nuclei, fraction of G2 and M nuclei, and RSG1. Four model formulations were tested; these models are not comprehensive of all possible models that could be tested but represent formulations 1) similar to previous linear models that used only cell cycle parameters to model growth rate (Theilacker and Shen, 2001; Domingos et al., 2012), and 2) take into account that the relationship between cell cycle covariates and growth rate may vary with either size or temperature. Two additive GAMs, representative of previous linear models, included all potential cell cycle covariates as well as either SL or the product of SL and BDA for the size covariate (BDA was used to take into account growth in body depth, and the product of SL and BDA is correlated with larval weight, van der Meeren, 1991; models 1 and 2, Table 2). SL and BDA could not be used as separate covariates in the same model because they were highly autocorrelated (r=0.96) resulting in multicollinearity in the model. Two variable coefficient GAMs (Bacheler et al., 2009) allowed the relationship between cell cycle covariates and growth rate to vary with either SL or temperature (models 3 and 4, Table 2). The two variable coefficient GAM formulations represented that the relationship between the cell cycle parameter and growth rate was linear (fraction of S-stage nuclei, fraction of G2-and-M-stage nuclei, and RSG1), but could vary with either SL (model 3, Table 2) or temperature (model 4, Table 2). Cell cycle parameters may vary with standard length for such reasons as larvae becoming better predators (i.e., improved

feeding, Porter et al., 2005), and increased digestive tract nutrient assimilation efficiency (Porter and Theilacker, 1999). For Walleye Pollock larvae the fraction of S-stage nuclei increases with temperature (Porter and Bailey, 2011), suggesting that temperature also affects the cell cycle. Backward stepwise variable selection based on Akaike Information Criterion (AIC) was used to select the covariates included in models. A covariate with a p-value > 0.05 was removed from the model and the model was rerun. The covariate was not included in the final model formulation if the AIC decreased upon its exclusion, but it was included if AIC increased. Residuals were visually assessed to check for normality and independence. R version 3.4.0 (R Core Team, 2017) and mgcv package (version 1.8-17; Wood, 2006) were used.

To determine the model that best predicted growth rates, the model formulations were compared using independent validation testing based on the following criteria: 1) how accurately the model predicted laboratory growth rates. This test compared predicted growth rate and corresponding laboratory growth rate for each larva to determine the model with the highest accuracy; 2) how well predicted growth rates followed somatic growth. The distance from the increment at first feeding to the otolith edge represents growth over the time period from first feeding to when the larva was captured. The Pearson correlation coefficient was calculated for the relationship between predicted growth rate and the distance from the first feeding increment to the otolith edge, and the model with the highest correlation would indicate that predictions tracked somatic growth better than the other models; and 3) similarity between predicted growth rates and otolith-derived growth rates. Otolith-derived growth rate is the most common method used to calculate growth rates of fish larvae in the field, and this test gives an indication of how comparable results from the two methods are. Model predicted and otolith-derived growth rate for the same larva can differ because otolith-derived growth rate uses the number of increments

from the first feeding mark to the otolith edge for the number of days from first feeding to capture, and the growth rate models use the first day when 50% of larvae were observed to be feeding as day of first feeding for determining number of days after first feeding a larva was at capture. Some larvae start feeding before and after day of 50% feeding and that will affect the calculation of growth rate. The testing data set consisted of 45 laboratory reared larvae that were not used in the formulation of the models ranging in SL from 6.42 to 8.63 mm from high and low prey density treatments from 1.6°, 3.2°, 6.1°, and 8.3°C (Table 3). A laboratory growth rate and a predicted growth rate from each model was calculated for each larva. Differences between laboratory growth rate and predicted growth rates among the models were compared using repeated measures ANOVA. Otolith-derived growth rate was calculated as the difference in length between the mean SL at first feeding for the corresponding temperature and feeding treatment and size of a larva at the time of capture, divided by the number increments from first feeding to the otolith edge. Differences between otolith-derived growth rate and predicted growth rates among the models were compared using repeated measures ANOVA. SYSTAT vers. 13 (SYSTAT software, inc., San Jose, CA) was used for all statistical testing.

The utility of using flow cytometry to classify larvae as fast- or slow-growing was investigated by formulating binomial GAMs with logit link function similar to the growth rate models. The rational was to compare accuracy of growth rate prediction (absolute growth rate) to growth rate classification to determine which method would be most useful for use in the field. For the response variable, each larva was determined to be fast or slow growing based on predicted SL from a linear regression of age and SL from the high prey density feeding treatment for each temperature. Only the high prey density treatment was used for that procedure because larvae in that treatment were most likely to have growth rates similar to healthy larvae in the

303 field. For a given sampling day, a larva less than predicted size for that day was identified as
304 slow-growing, and a larva equal to or greater than that size was fast-growing. Growth
305 classification models predicted the probability of fast growth, and were formulated using the
306 same stepwise procedure described for the growth rate models. The validation testing set was
307 used to determine the model that most accurately classified larvae as fast- or slow-growing.
308 *1.5 Walleye Pollock larvae growth rate in the western Gulf of Alaska*
309 Walleye Pollock larvae were opportunistically sampled from the Gulf of Alaska near Kodiak
310 Island, and from the area between the Shumagin Islands and the southern end of Kodiak Island
311 from 18-30 May 2013 during an ichthyoplankton survey conducted by the Alaska Fisheries
312 Science Center (Fig. 1). Collections were made using a 60 cm bongo frame fitted with 505-µm
313 mesh nets towed obliquely to a depth of 100 m or 10 m off bottom, whichever was shallower.
314 Water temperature was measured during each tow using a Sea-Bird SBE 19 Plus SeaCat attached
315 to the towing wire. At completion of a tow, Walleye Pollock larvae were immediately removed
316 from the net codend, placed onto a microscope slide with chilled seawater, imaged with a digital
317 camera and individually frozen at -80ºC. Mean temperature between the surface and 50 m depth
318 was used as the value for temperature in the growth model because most Walleye Pollock larvae
319 in Shelikof Strait, Gulf of Alaska are located at this depth interval (Kendall et al., 1994).
320 Temperature, SL, transformed fractions of S-stage nuclei, G2-and-M stage-nuclei, and RSG1
321 were used to predict a growth rate for each larva at a station, and to classify them as fast- or
322 slow-growing. The mean growth rate and mean probability of fast growth of larvae at a station
323 were used as the value for that station. A mean otolith-derived growth rate was also calculated
324 for each station. Size at first feeding was estimated from a linear regression of age and size of
325 Walleye Pollock larvae from Shelikof Strait for 1983-2001 from hatching to 35 days after

hatching (n = 4159; A. Dougherty unpublished data). Mean predicted SL of larvae 5, 6, and 7 days after hatching was used as the size at first feeding (5.49 mm) because those ages represent the time when larvae typically begin feeding at the temperatures measured in the study area. Mean model predicted growth rates and otolith-derived growth rates for each station were compared using the paired t-test.

Results

2.1 Growth model formulation

Linear regressions of SL and days after first feeding for the high prey density treatments at 1.6°, 3.0°, 3.2°, 6.1°, and 8.3°C showed that growth rates were 0.08, 0.09, 0.09, 0.18, and 0.18 mm d^{-1}, respectively. Those growth rates indicate that larvae grew well when compared to results from previous rearing experiments at approximately the same temperatures (0.04, 0.06, 0.14, 0.16 mm d^{-1} for 1.4°, 3.2°, 5.9°, 9.0°C, respectively; S. Porter unpublished data). Additionally, 9 larvae age-22 days after first feeding, reared at 2.8°C and fed high prey density were included to increase the number of older larvae for temperatures near 3°C. A total of 318 larvae ranging in SL from 5.32 to 11.17 mm were used to formulate the models (Table 3). The 1.6°, 3.0°, 3.2°, and 8.3°C treatments had no larvae remaining after three sampling dates (Table 3).

Models 1, 3, and 4 produced nearly identical r^2 values and similar AIC values, indicating that these models fit the data similarly (Table 2). Model 2 had the largest AIC and smallest r^2 value for the four models tested and was not considered further (Table 2). Models 1 and 3 included all covariates, and model 4 covariates were SL, and the effects of G2-and-M, and S varying with temperature (Table 2). Other covariates (rearing temperature alone, and RSG1) were not included in this model because they were not significant and did not decrease the AIC score.

Predicted growth rates from models 1, 3, and 4 resulting from the independent validation data set were compared to the corresponding laboratory growth rate, correlation with the distance between the first feeding increment and the otolith edge, and to otolith-derived growth rates to determine the model that most accurately predicted growth rates. Overall, predictions from all models were correlated with laboratory growth rates (Fig. 2a, b, c; Table 4). The slopes of linear regressions for the relationship between laboratory and predicted growth rates among models were not significantly different showing that all models predicted growth rate similarly (ANCOVA, $p = 0.35$; Fig. 2a, b, c; Table 4). Mean predicted growth rate for each model was not significantly different from laboratory growth rate for rearing temperatures 1.6°, and 8.3°C (repeated measures ANOVA, $p > 0.05$; Table 5). For 3.2° and 6.1°C, mean predicted growth rates were significantly different from mean laboratory growth rates (repeated measures ANOVA, $p < 0.01$; Table 5). Growth rate was significantly overestimated by each model for 3.2°C, and for 6.1°C all models significantly underestimated growth rate (Table 5). Overall mean percent error between predicted and laboratory growth was similar among models, 23% for models 1 and 4, and 24% for model 3. Model 1 had the highest percentage of accurate predictions (i.e., predicted growth rate of a larva was equal to the corresponding laboratory growth rate; 16%, Table 4), and this model also had the highest percentage of laboratory growth rates that fell within the 95% confidence interval of the predictions (33%; Table 4).

A subset of larvae from the independent validation data set were used for model assessment involving otolith microstructure analysis ($n = 19$). Larvae reared at 1.6° and 3.2°C were excluded because of either increment compression (1.6°C) or non-daily increment deposition (3.2°C) that made determination of the number of daily increments and measurement of the distance from the first feeding increment to otolith edge unreliable. Model 1 predictions had the highest correlation

372 with the distance between the first feeding increment and the otolith edge indicating that this
373 model had better fit with somatic growth than the other models (Table 6). Mean otolith-derived
374 growth rate was significantly greater and model 1 and 3 predicted growth rates were significantly
375 less than mean laboratory growth rate (repeated measures ANOVA, $p < 0.01$; Table 6). The
376 percentage of otolith-derived growth rates that were within the 95% confidence interval of the
377 predictions of each model was 11% (2/19), 5% (1/19), and 16% (3/19) for models 1, 3, and 4,
378 respectively (Table 6).

379 Of the models tested, model 1 was chosen as the best model for predicting Walleye Pollock
380 larvae laboratory growth rate (i.e., growth from first feeding). This model showed that increasing
381 temperature had a positive effect on growth over the range of temperatures tested (Fig. 3a), and
382 also indicated that larvae smaller than approximately 6.5 mm SL grew slower than larger larvae,
383 most likely because the smaller size range included starving larvae and larvae that were just
384 beginning to feed (Fig. 3b). Higher growth rates were associated with increasing values of the
385 fraction of G2-and-M-stage nuclei, and fraction of S-stage nuclei (Fig. 4a, b). The effect of
386 RSG1 on growth rate was weak for large ratios as evidenced by the wide 95% confidence
387 interval for those ratios (Fig. 4c). This model had both the highest percentage of correct
388 predictions and the highest percentage of laboratory growth rates that fell within the 95%
389 confidence interval of the predictions for the independent validation testing set (Table 4).
390 Additionally, correlation between growth rate predictions and the distance between the first
391 feeding increment and the otolith edge was highest with model 1 (Table 6). The percentage of
392 otolith-derived growth rates that were within the 95% confidence interval of the predicted values
393 of model 1 was nearly equal to that of model 4 (Table 6).

394 *2.2 Classification of growth*

Three binomial GAMs for classifying larvae as slow- or fast-growing, similar in formulation to growth models 1, 3, and 4 (growth classification models 1, 2, and 3, respectively; Table 7) were tested using the independent validation data set. The models predicted the probability of fast growth, and a larva with a probability ≥ 0.50 was classified as fast-growing. Growth classification models 1 and 3 had identical results with an accuracy of 69% (Table 7), and both more accurately classified fast-growing (82%) versus slow-growing larvae (57%). Growth classification model 2 was slightly more accurate overall (71%; Table 7), correctly classifying one additional slow-growing larva than the other two models and was chosen as the best growth classification model based upon highest overall accuracy. Model 2 indicated that larvae larger than approximately 9.5 mm were more likely to be fast growing than smaller sizes (Fig. 5), possibly because by the time larvae reach that size most individuals in poor condition (slow growing) have died. In general, cell cycle covariates had a strong influence on the probability of small larvae being fast growing and had a lesser effect on large larvae (Fig. 6a, b).

2.3 Comparing predicted and otolith-derived growth rates of western Gulf of Alaska Walleye Pollock larvae

Thirty-one larvae ranging in size from 5.91 to 14.91 mm SL were analyzed from 14 stations: 6 stations were located in the vicinity of Kodiak Island and 8 stations were in the area between Kodiak Island and the Shumagin Islands (Table 8, Fig. 1). One to four larvae were analyzed at each station, and otolith microstructure analysis was completed on all larvae except for the larva from station 187. Poor increment definition of those otoliths prevented the increments from being reliably counted. Predicted growth rates were highly correlated with the distance from the first-feeding increment to the otolith edge ($r = 0.98$), indicating that predicted rates were related to somatic growth. Overall, predicted and otolith-derived growth rates were not significantly

different from each other (0.21 ± 0.08 mm d^{-1} and 0.18 ± 0.01 mm d^{-1} respectively; paired t-test, p = 0.31). However, the greatest differences between predicted and otolith-derived growth rates were consistently at stations where mean larvae size was > 11 mm SL (stations 161, 162, 164, and 191; Table 8). For those stations, predicted growth rates were significantly higher than otolith-derived growth rates (0.31 ± 0.04 mm d^{-1} and 0.17 ± 0.005 mm d^{-1} respectively; paired t-test, p = 0.009; Table 8), and were also higher (range 0.26 to 0.36 mm d^{-1}) than the range of published values for Shelikof Strait larvae calculated using otolith microstructure analysis (0.14 to 0.24 mm d^{-1}; Bailey et al., 1996). A contributing factor to the large discrepancy in growth rates between the two methods for larvae > 11 mm SL may be that the growth model was formulated using larvae between 5.32 and 11.17 mm SL (only one larvae larger than 11 mm was used), so growth rates were predicted outside of the range of sizes used in the model causing growth to be overestimated. Additionally, no transforming larvae were included in the growth model, and Walleye Pollock larvae growth rate changes when they begin juvenile transformation about 12 mm SL (Brown et al., 2001). Predicted growth rates for stations where mean larvae size was ≤ 11 mm were not significantly different from otolith-derived growth rates (0.16 ± 0.04 mm d^{-1} and 0.19 ± 0.01 mm d^{-1} respectively; paired t-test, p = 0.15), and nearly all of the predicted rates were within the range of published values for Shelikof Strait larvae (Table 8). For this smaller size range, at stations where more than one larva was analyzed, mean otolith-derived growth rates were within the 95% confidence interval of the mean predicted growth rates for 6 out of 7 stations, and the mean percent error between the predicted and otolith-derived growth was 20%, much lower than 80% for larvae larger than 11 mm in size. Based on these results, the model appears to be most appropriate for larvae ≤ 11 mm, and this equates to about the first 4 weeks of feeding based on temperatures that typically occur at depths where Walleye Pollock larvae

441 reside. Larvae at all stations except for station 78 were classified as fast-growing (i.e., probability
442 of fast growth ≥ 0.50; Table 8). The predicted growth rate at station 78 was 0.14 mm d^{-1}, and that
443 corresponds with the lower end of the range of published growth rates (Bailey et al., 1996)
444 supporting that those larvae were growing slowly. There was a discrepancy between predicted
445 growth rate and growth classification for stations 18 and 187 because both stations were
446 classified as fast-growing but predicted growth rates were the slowest of all the stations (Table
447 8).
448
449 Discussion
450 The growth model developed in this study represents an improvement over other models that
451 have used flow cytometric cell cycle analysis to predict growth rates of fish larvae (Theilacker
452 and Shen, 2001; Domingos et al., 2012). Cell cycle covariates, larval length, and temperature
453 accounted for 79% of the variance used to predict growth rate of Walleye Pollock larvae in our
454 study. Previous models used only cell cycle covariates and explained about 55% of the variance
455 in growth rate and were based on only one temperature, so they may be better suited for
456 application in the laboratory rather than to the field. Growth rate of larvae reared in the high prey
457 density treatment at 6.1°C (0.18 mm d^{-1}) was within the range of growth rates for Gulf of Alaska
458 Walleye Pollock larvae at similar temperature (Bailey et al., 1996) supporting that predicted
459 growth rates should reflect growth in the field. A laboratory study that reared Walleye Pollock
460 larvae at 0°, 2°, 5°, and 12°C reported that larvae grew fastest (% mass day^{-1}) at the highest
461 temperature tested, and survival was highest at 2°C and lowest at 12°C (Koenker et al., 2018).
462 Survival at 5°C was nearly equal to survival at 2°C (Koenker et al., 2018) suggesting that the
463 optimal temperature range for survival in the field may be 2° to 5°C. The optimal temperature for

Walleye Pollock larvae growth is not consistent among studies. In our study growth rate at 6.1° and 8.3°C was alike indicating that a temperature threshold may have been reached, and other studies have found no significant difference in growth between 7.4° and 9.9°C (Porter and Bailey 2007) or that growth rate continued to increase up to 12°C (Koenker et al., 2018). The growth model produced reasonable results when applied to Gulf of Alaska larvae ≤ 11 mm SL as shown by predicted growth rates within the range of published values for larvae in that area. Confirmation of the growth model's utility is shown for the larva at station 187 (Table 8). The otoliths of that larva were unreadable due to poor increment definition so the otolith aging method could not be used to calculate growth rate. In this circumstance, the predicted growth rate was 0.05 mm d^{-1} (Table 8) indicating slow growth. Poor increment definition can be an indication of weak growth (A. Dougherty, pers. comm.), supporting the model prediction.

The model for classifying larvae as fast- or slow-growing had a somewhat lower overall classification accuracy (71%) than a logistic regression model developed for Walleye Pollock larvae using the sum of the fractions of nuclei in S-stage and G2-and M-stages, and standard length as covariates (79%; Theilacker and Shen, 2001). The difference in classification accuracy between these models may be due, in part, because the Theilacker and Shen model was tested with the same data used to formulate it. In that case, classification accuracy would likely be higher compared to using an independent data set as was done here. Flow cytometric cell cycle analysis may be better suited for classifying larvae as fast- or slow-growing rather than predicting absolute growth rates because the accuracy of the growth classification model was higher than the growth rate model. Thirty-three percent of laboratory growth rates of the test set larvae were within the 95% confidence interval of the predicted growth rates compared to 71% of larvae being correctly classified as fast- or slow-growing. Growth rate predictions and growth

487 classification for late-stage, field-collected Walleye Pollock larvae would be improved by adding
488 larvae as large as 15 mm to the models to encompass the range of sizes of larvae collected during
489 spring ichthyoplankton surveys conducted in the Bering Sea or Gulf of Alaska.

490 Differences among predicted, laboratory, and otolith-derived growth rates for the same larva
491 may be partially due to how age and size at day of the start of exogenous feeding (first feeding)
492 was determined. Day of first feeding was defined for this study as the day when 50% of the
493 larvae were observed to have started feeding, and the mean SL for each treatment on this day
494 was used as size at first feeding. The initiation of first feeding for Walleye Pollock larvae in the
495 laboratory generally occurs over a 3-day period (Porter and Theilacker, 1999). Larvae that start
496 feeding at the beginning of this period would be younger and most likely smaller than the mean
497 length at 50% feeding; larvae that start feeding near the end of the first feeding period would be
498 older and possibly larger than the mean. This variation in the onset of feeding can affect
499 calculation of growth rates. For example, larvae from the 6°C independent validation test set
500 were classified as age 13 days after first feeding based on the day when 50% of the larvae started
501 feeding. Otolith increment counts of that group of larvae ranged from 10 to 15 days after first
502 feeding, indicating that some larvae began feeding five days earlier than others. This range in age
503 when feeding actually began will cause differences between predicted growth rates (that are
504 based on age beginning when 50% of the larvae started feeding), and otolith-derived growth
505 rates that use the number of increments from first feeding to the otolith edge for age.
506 Additionally, flow cytometric cell cycle analysis can detect differences between starved and fed
507 fish larvae after 1 to 3 days of starvation (Theilacker et al., 1996; Catalán et al., 2007; Porter and
508 Bailey, 2011), indicating that cell cycle stages may be more related to recent growth rate (i.e.,

509 growth within the last 1 to 3 days before capture) rather than growth rate from first feeding to
510 capture that the otolith-derived growth rates represented in our study.

511 The recruitment process of Walleye Pollock is initiated at the egg and larval stage, with larval
512 survival being a critical first step. Variability in growth rate during early life can affect the
513 survival of larvae due to size-dependent mortality (Leggett and DeBlois, 1994), and that can
514 potentially affect year class strength. The abundance of Walleye Pollock larvae reaching 15 mm
515 SL was positively related (although not statistically significant) to recruitment for years 1979 to
516 1991 (Bailey et al., 2012). In our study, the models worked best for larvae during the period of
517 about the first 4 weeks of feeding, and studies indicate that growth early in the larval period may
518 have a more significant effect on survival than growth later in this period. For example, field
519 studies have shown that for a shallow-water reef fish the Rainbow Wrasse, *Coris julis*, size at age
520 30 days was positively correlated with recruitment (Fontes et al., 2011). For King George
521 Whiting, *Sillaginodes punctate*, larvae, growth from hatching to 25 - 30 days was the most
522 critical period for survival (Jenkins and King, 2006). Flow cytometric cell cycle analysis offers
523 promise as an alternative method for determining growth rate of fish larvae when otolith daily
524 increments cannot be reliably counted.

525

526 Acknowledgments

527 M. Canino, A. Deary, J. Duffy-Anderson, and L. Rogers provided helpful comments on early
528 drafts of the manuscript. This research was funded by the North Pacific Research Board (NPRB
529 grant no. 1417) and the Alaska Fisheries Science Center. It is contribution EcoFOCI-0913 to
530 NOAA's Ecosystems and Fisheries-Oceanography Coordinated Investigations. The findings and
531 conclusions in the paper are those of the authors and do not necessarily represent the views of the

National Marine Fisheries Service, NOAA. Reference to trade names does not imply endorsement by the National Marine Fisheries Service, NOAA.

534 References

535 Akimova, A., Hufnagl, M., Kreus, M., Peck, M.A., 2016. Modeling the effects of temperature on
536 the survival and growth of North Sea cod (*Gadus morhua*) through the first year of life.
537 Fish. Oceanogr. 25, 193-209.
538
539 Anderson, J.T., 1988. A review of size dependent survival during pre-recruit stages of fishes in
540 relation to recruitment. J. Northwest Atl. Fish. Sci. 8, 55–66.
541
542 Bacheler, N.M., Bailey, K.M., Ciannelli, L., Bartolino, V., Chan, K.-S., 2009. Density
543 dependent, landscape, and climate effects on spawning distribution of walleye pollock
544 *Theragra chalcogramma*. Mar. Ecol. Progr. Ser. 391, 1–12.
545
546 Bailey, K.M., Stehr, C.L., 1988. The effects of feeding periodicity and ration on the rate of
547 increment formation in otoliths of larval walleye pollock *Theragra chalcogramma*
548 (Pallas). J. Exp. Mar. Biol. Ecol. 122, 147-161.
549
550 Bailey, K.M., Spring S., 1992. Comparison of larval, age-0 juvenile and age-2 recruit abundance
551 indices of walleye pollock *Theragra chalcogramma* in the western Gulf of Alaska. ICES
552 J. Mar. Sci. 49, 297−304.
553
554 Bailey, K.M., Brown, A.L., Yoklavich, M.M., Mier, K.L., 1996. Interannual variability in
555 growth of larval and juvenile walleye pollock *Theragra chalcogramma* in the western
556 Gulf of Alaska. Fish. Oceanogr. 5(Suppl. 1), 137-147.

Brown, A.L., Busby, M.S., Mier, K.L., 2001. Walleye pollock *Theragra chalcogramma* during transformation from the larval to juvenile stage: Otolith and osteological development. Mar. Biol. 139, 845-851.

Buckley, L.J., Caldarone, E.M., Clemmesen, C., 2008. Multi-species larval fish growth model based on temperature and fluorometrically derived RNA/DNA ratios: Results from a meta-analysis. Mar. Ecol. Progr. Ser. 371, 221–232.

Caldarone, E.M., St. Onge-Burns, J.M., Buckley, L.J., 2003. Relationship of RNA/DNA ratio and temperature to growth in larvae of Atlantic cod *Gadus morhua.* Mar. Ecol. Progr. Ser. 262, 229–240.

Caldarone, E.M., 2005. Estimating growth in haddock larvae *Melanogrammus aeglefinus* from RNA:DNA ratios and water temperature. Mar. Ecol. Progr. Ser. 293, 241–252.

Campana, S.E., 1996. Year-class strength and growth rate in young Atlantic cod *Gadus morhua*. Mar. Ecol. Progr. Ser. 135, 21-26.

Catalán, I.A., Berdalet, E., Olivar, M.P., Roldán, C., 2007. Response of muscle-based biochemical condition indices to short-term variations in food availability in post-flexion reared sea bass *Dicentrarchus labrax* (L.) larvae. J. Fish Biol. 70, 391-405.

Chambers, R.C., Leggett, W.C., 1987. Size and age at metamorphosis in marine fishes: an Analysis of laboratory-reared winter flounder (*Pseudopleuronectes americanus*) with a review of variation in other species. Can. J. Fish. Aquat. Sci. 44, 1936–1947.

Domingos, J.A., Fromm, P., Smith-Keune, C., Jerry, D.R., 2012. A robust flow-cytometric protocol for assessing growth rate of hatchery-reared barramundi *Lates calcarifer* larvae. J. Fish Biol. 80, 2253-2266.

Dougherty, A.B., 2008. Daily and sub-daily otolith increments of larval and juvenile walleye pollock, *Theragra chalcogramma* (Pallas), as validated by alizarin complexone experiments. Fish. Res. 90, 271-278.

Fontes, J., Santos, R.S., Afonso, P., Caselle, J.E., 2011. Larval growth, size, stage duration and recruitment success of a temperate reef fish. J. Sea Res. 65, 1-7.

Hare, J.A., Cowen, R.K., 1997. Size, growth, development, and survival of the planktonic larvae of *Pomatomus saltatrix* (Pisces: Pomatomidae). Ecol. 78, 2415–2431.

Heintz, R.A., Vollenweider, J.J., 2010. Influence of size on the sources of energy consumed by overwintering walleye pollock (*Theragra chalcogramma*). J. Exp. Mar. Biol. Ecol. 393, 43-50.

603 Houde, E.D., 1987. Fish early life dynamics and recruitment variability. Am. Fish. Soc. Symp.
604 2, 17–29.
605
606 Hunt, G. L., Coyle, K. O., Eisner, L. B., Farley, E. V., Heintz, R. A., Mueter, F., Napp, J. M.,
607 Overland, J. E., Ressler, P. H., Salo, S., Stabeno, P. J. 2011. Climate impacts on eastern
608 Bering Sea foodwebs: a synthesis of new data and an assessment of the Oscillating
609 Control Hypothesis. ICES J. Mar. Sci. 68, 1230-1243.
610
611 Jenkins, G.P., King, D., 2006. Variation in larval growth can predict recruitment of a temperate,
612 seagrass-associated fish. Oecology 147, 641-649.
613
614 Kendall, A.W., Jr., Incze, L.S., Ortner, P.B., Cummings, S.R., Brown, P.K., 1994. The vertical
615 distribution of eggs and larvae of walleye pollock, *Theragra chalcogramma,* in Shelikof
616 Strait, Gulf of Alaska. Fish. Bull., U.S. 92, 540-554.
617
618 Koenker, B. L., Laurel, B. J., Copeman, L. A., Ciannelli, L., 2018. Effects of temperature and
619 food availability on the survival and growth of larval Arctic cod (*Boreogadus saida*) and
620 walleye pollock (*Gadus chalcogrammus*). ICES J. Mar. Sci. 75, 2386–2402.
621
622 Meekan, M., Fortier, L. 1996. Selection for fast growth during the larval life of Atlantic cod
623 *Gadus morhua* on the Scotian shelf. Mar. Ecol. Prog. Ser. 137, 25–37.
624
625 Murray, A., Hunt, T., 1993. The cell cycle: an introduction. Oxford Univ. Press, Inc., New York,

251 p.

Porter, S.M., Theilacker, G.H., 1996. Larval walleye pollock, *Theragra chalcogramma*, rearing techniques used at the Alaska Fisheries Science Center, Seattle, Washington. Processed Rep. 96-06, 26 p. Alaska Fish. Sci. Cent., NOAA, Natl. Mar. Fish. Serv., 7600 Sand Point Way NE, Seattle, WA 98115-0070.

Porter, S.M., Theilacker, G.H., 1999. The development of the digestive tract and eye in larval walleye pollock, Theragra chalcogramma. Fish. Bull., U.S. 97:722-729.

Porter, S.M., Ciannelli, L., Hillgruber, N., Bailey, K.M., Chan, K-S, Canino, M.F., and Haldorson, L.J., 2005. Environmental factors influencing larval walleye pollock *Theragra chalcogramma* feeding in Alaskan waters. Mar. Ecol. Progr. Ser. 302: 207-217.

Porter, S.M., Bailey, K.M., 2007. Optimization of feeding and growth conditions for Walleye Pollock *Theragra chalcogramma* (Pallas) larvae reared in the laboratory. AFSC Processed Rep. 2007-06, 20 p. Alaska Fish. Sci. Cent., NOAA, Natl. Mar. Fish. Serv., 7600 Sand Point Way NE, Seattle, WA 98115-0070.

Porter, S.M., Bailey, K.M., 2011. Assessing the condition of walleye pollock *Theragra chalcogramma* (Pallas) larvae using muscle-based flow cytometric cell cycle analysis. J. Exp. Mar. Biol. Ecol. 399, 101-109.

649 Porter, S.M., Bailey, K.M., 2013. Using measurements of muscle cell nuclear RNA with flow
650 cytometry to improve assessment of larval condition of walleye pollock (*Gadus*
651 *chalcogrammus*). Fish. Bull., U.S. 111, 337-351.
652
653 R Core Team, 2017. R: A Language and Environment for Statistical Computing. R Foundation
654 for Statistical Computing, Vienna, Austria.
655
656 Rice, J.A., Miller, T.J., Rose, K.A., Crowder, L.B., Marschall, E.A., Trebitz, A.S., DeAngelis,
657 D.L., 1993. Growth rate variation and larval survival: inferences from an individual-
658 based size-dependent predation model. Can. J. Fish. Aquat. Sci. 50, 133–142.
659
660 Stabeno, P.J., Kachel, N.B., Moore, S.E., Napp, J.M., Sigler, M., Yamaguchi, A., Zerbini, A.N.,
661 2012. Comparison of warm and cold years on the southeastern Bering Sea shelf and some
662 implications for the ecosystem. Deep-sea Res. II 65-70, 31-45.
663
664 Takasuka, A., Aoki, I., Mitani, I., 2003. Evidence of growth-selective predation on larval
665 Japanese anchovy *Engraulis japonicus* in Sagami Bay. Mar. Ecol. Progr. Ser. 252, 223–
666 238.
667
668 Takasuka, A., Aoki, I., Mitani, I., 2004. Three synergistic growth-related mechanisms in the
669 short-term survival of larval Japanese anchovy *Engraulis japonicus* in Sagami Bay. Mar.
670 Ecol. Progr. Ser. 270, 217-228.
671

672 Theilacker, G.H., Bailey, K.M., Canino, M.F., Porter, S.M., 1996. Variations in larval walleye
673 pollock feeding and condition: a synthesis. Fish. Oceanogr. 5(Suppl. 1), 112-123.
674
675 Theilacker, G.H., Shen, W., 2001. Evaluating growth of larval walleye pollock, *Theragra*
676 *chalcogramma*, using cell cycle analysis. Mar. Biol. 135, 897-907.
677
678 van der Meeren, T., 1991. Selective feeding and prediction of food consumption in turbot larvae
679 (*Scophthalmus maximus* L.) reared on the rotifer *Brachionus plicatilis* and natural
680 zooplankton. Aquaculture 93, 35-55.
681
682 Ware, D.M., 1975. Relation between egg size, growth, and natural mortality of larval fish. J.
683 Fish. Res. Bd. Can. 32, 2503–2512.
684
685 Watson, S., Allan, B.J.M, McQueen, D.E., Nicol, S., Parsons, D. M., Pether, S.M.J., Pope, S.,
686 Setiawan, A.N., Smith, N., Wilson, C., Munday, P.L., 2018. Ocean warming has a greater
687 effect than acidification on the early life history development and swimming performance
688 of a large circumglobal pelagic fish. Glob. Change Biol. 24, 4368-4385.
689
690 Wood, S.N., 2006. Generalized additive models: an introduction with R. Chapman and
691 Hill/CRC, Boca Raton, FL, 392 p.
692

Figure Captions

Figure 1. Sampling stations where Walleye Pollock larvae (*Gadus chalcogrammus*) were collected in the Gulf of Alaska in May 2013.

Figure 2. Relationship between laboratory and predicted growth rate for models 1 (a), 3 (b), and 4 (c).

Figure 3. Partial effects of temperature (°C; a) and standard length (mm; b) on growth rate (mm d^{-1}) of Walleye Pollock larvae (*Gadus chalcogrammus*) for growth model 1. Tick marks on X-axis show either rearing temperatures or individual standard length measurements. The 95% confidence interval is shown by dashed lines.

Figure 4. Partial effects of fraction of G2-and-M-stage nuclei (a), fraction of S-stage nuclei (b), and ratio of the number of S-stage nuclei to the number of G1-stage nuclei with high RNA content (c) on growth rate (mm d^{-1}) of Walleye Pollock (*Gadus chalcogrammus*) larvae for growth model 1. Cell cycle data were normalized using the arcsin $\sqrt{x}$ transformation. Tick marks on X-axis show individual measurements. The 95% confidence interval is shown by dashed lines.

Figure 5. Partial effect of standard length (mm) on the probability of fast growth of Walleye Pollock (*Gadus chalcogrammus*) larvae for growth classification model 2. Tick marks on X-axis show individual measurements. Y-axis represents values that larval size contributes to predicted probability of fast growth. The 95% confidence interval is shown by dashed lines.

716 Figure 6. Partial effects of standard length (SL, mm) and fraction of G2-and-M-stage nuclei (a),
717 and SL and fraction of S-stage nuclei (b) on the probability of fast growth of Walleye Pollock
718 (*Gadus chalcogrammus*) larvae for growth classification model 2. Cell cycle data were
719 normalized using the arcsin $\sqrt{x}$ transformation. Grey scale shows probability of fast growth
720 increasing from dark to light colors. Contour lines indicate probability of fast growth.

721 Fig.1

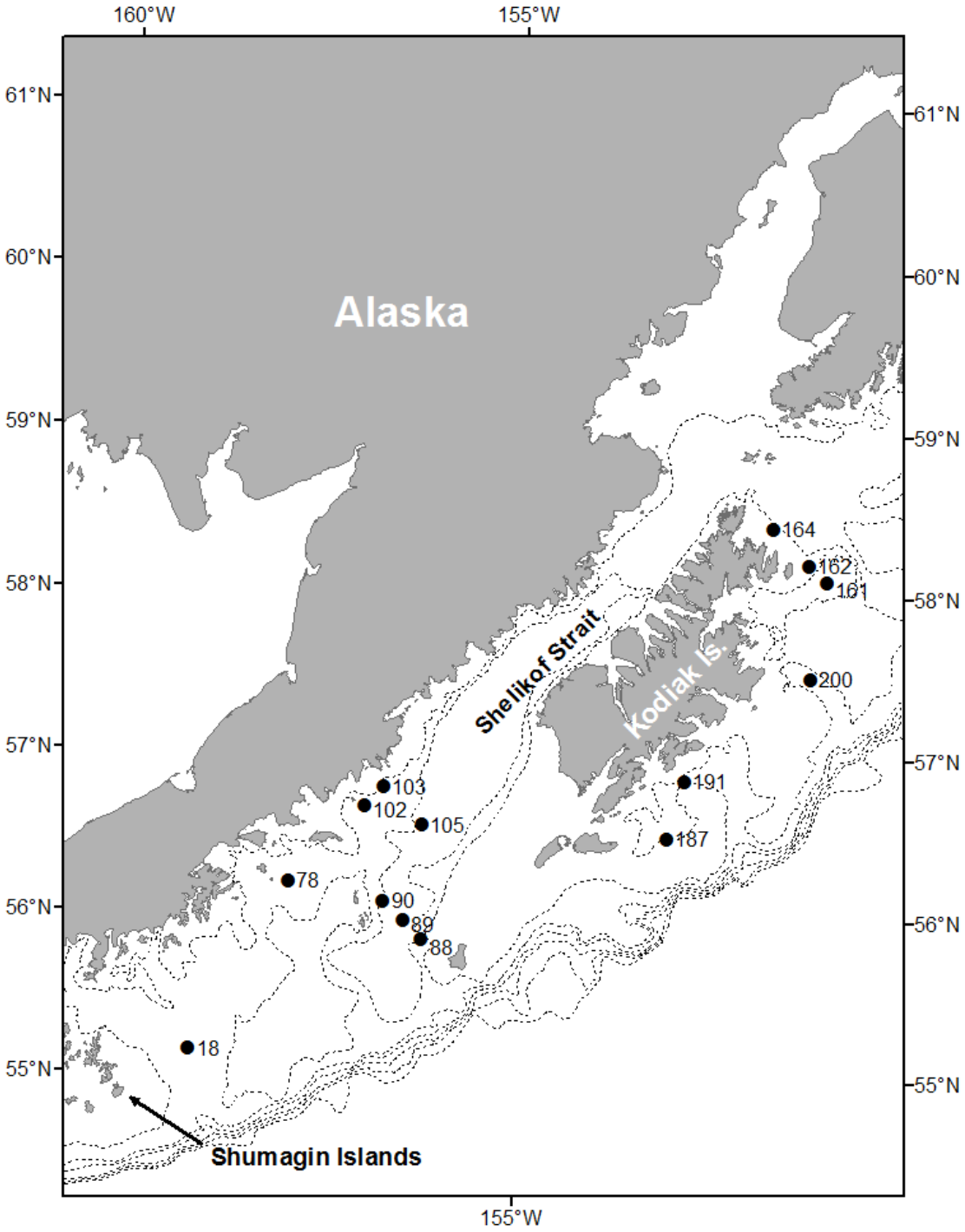
160°W
155°W
61°N
60°N
59°N
58°N
57°N
56°N
55°N
Alaska
Shelikof Strait
Kodiak Is.
164
162
161
200
191
187
103
102
105
78
90
89
88
18
Shumagin Islands

722

723 Fig. 2

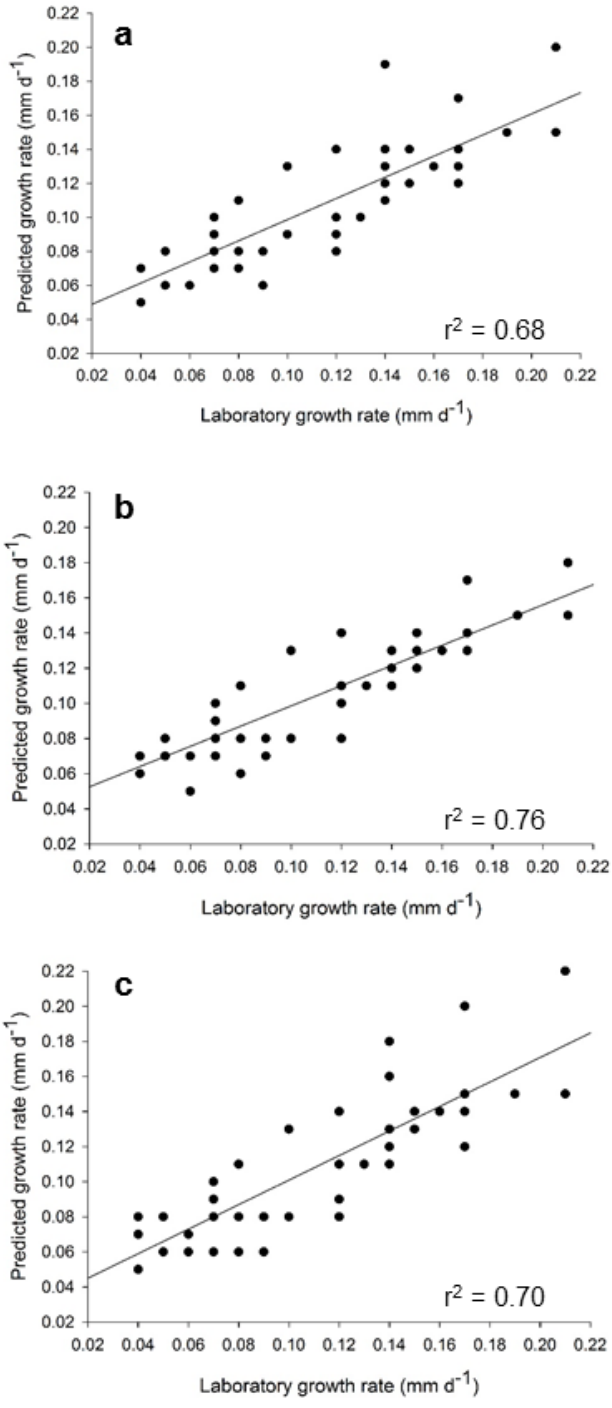
a
Predicted growth rate (mm d-1)
Laboratory growth rate (mm d-1)
r2 = 0.68
b
Predicted growth rate (mm d-1)
Laboratory growth rate (mm d-1)
r2 = 0.76
c
Predicted growth rate (mm d-1)
Laboratory growth rate (mm d-1)
r2 = 0.70

724

725 Fig. 3

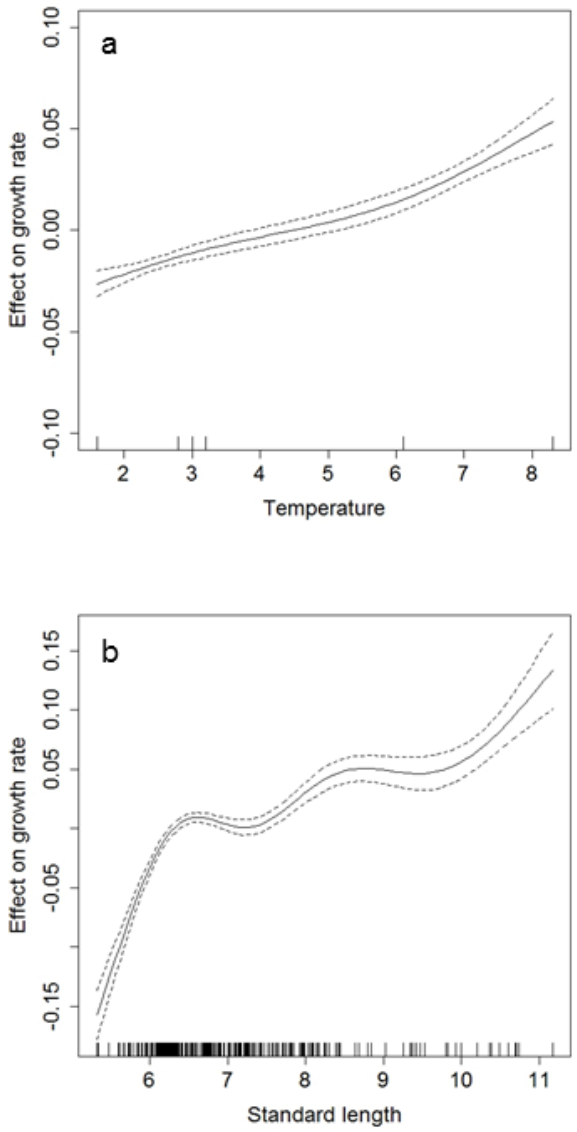
a
Effect on growth rate
0.10
0.05
0.00
-0.05
-0.10
2
3
4
5
6
7
8
Temperature
b
Effect on growth rate
0.15
0.10
0.05
-0.05
-0.15
6
7
8
9
10
11
Standard length

726

727 Fig. 4

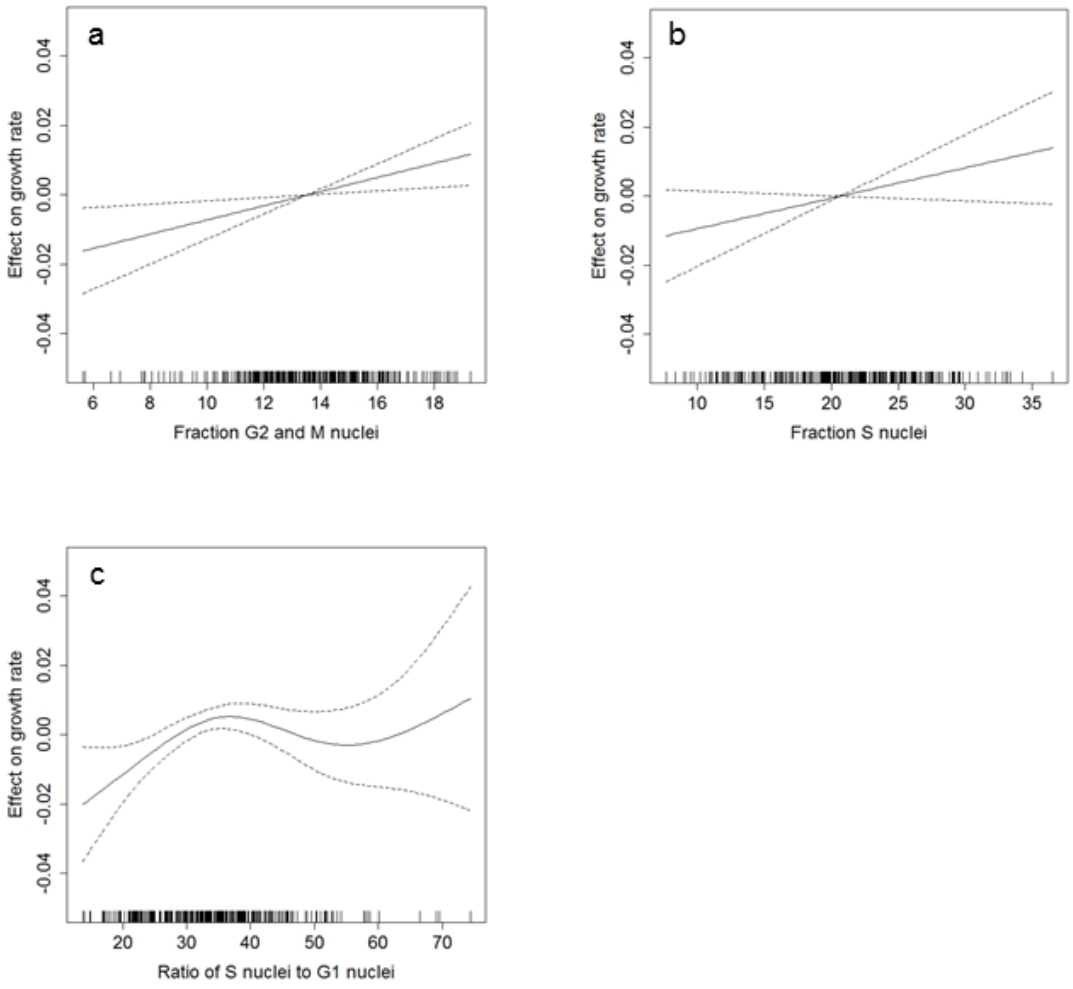
a
Effect on growth rate
0.04
0.02
0.00
-0.02
-0.04
6
8
10
12
14
16
18
Fraction G2 and M nuclei
b
Effect on growth rate
0.04
0.02
0.00
-0.02
-0.04
10
15
20
25
30
35
Fraction S nuclei
c
Effect on growth rate
0.04
0.02
0.00
-0.02
-0.04
20
30
40
50
60
70
Ratio of S nuclei to G1 nuclei

728

729 Fig. 5

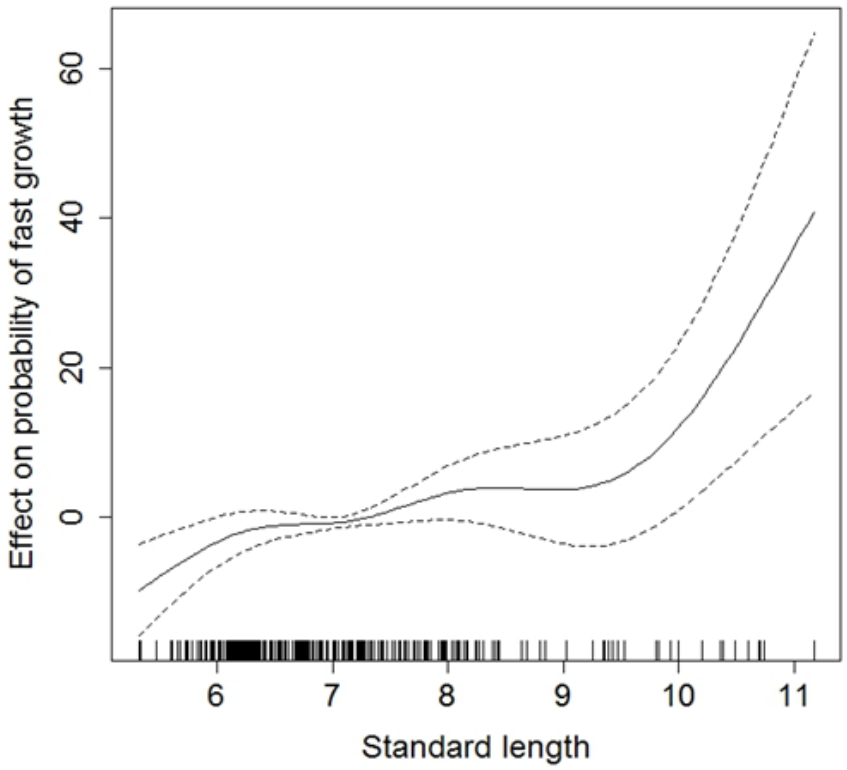
Effect on probability of fast growth
0
20
40
60
6
7
8
9
10
11
Standard length

730

731 Fig. 6

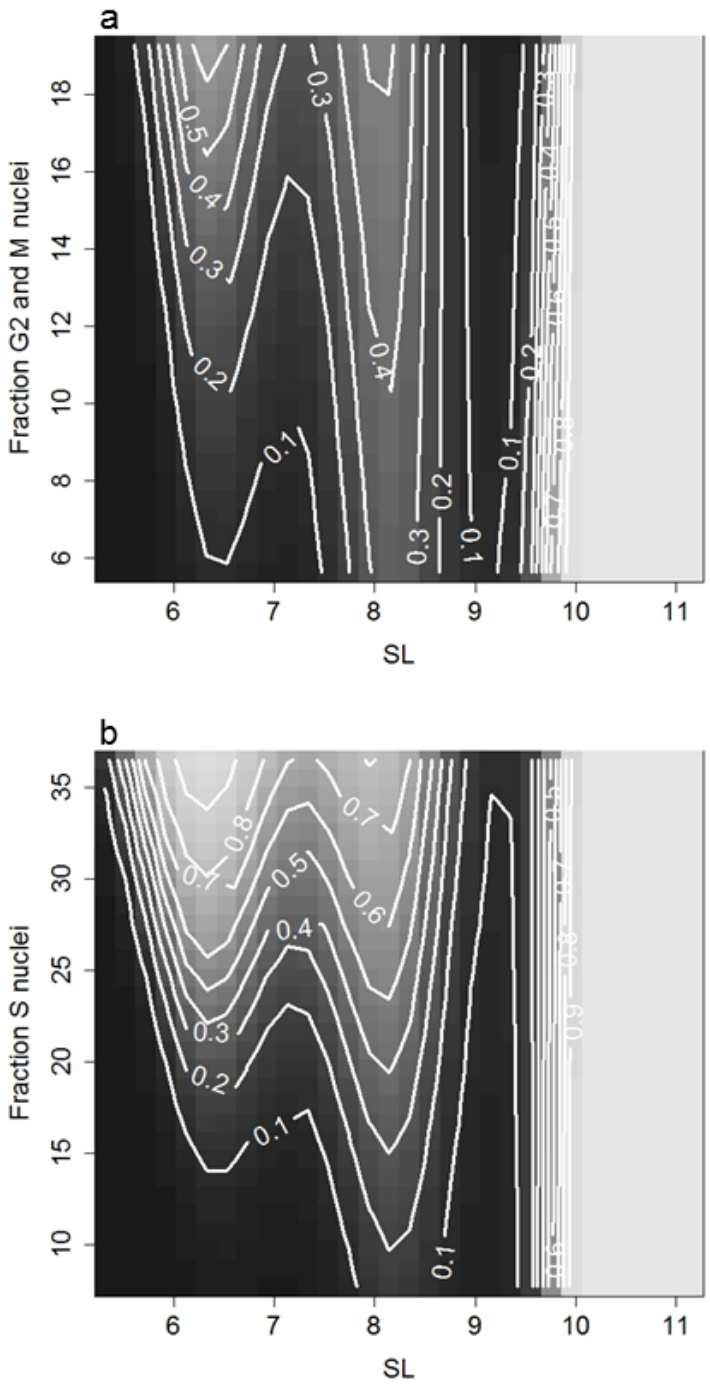

732

733 Table 1. Experimental year, rearing temperature, and feeding treatments for Walleye Pollock
734 (*Gadus chalcogrammus*) larvae laboratory studies used to formulate the growth model.
735

Year	Temperature ± SD[a] (°C)	Feeding treatments[b]
2014	3.2 ± 0.1	HP, LP, UF
2014	6.1 ± 0.4	HP, LP, UF
2015	1.6 ± 0.1	HP, LP, UF
2015	3.0 ± 0.1	S6F, F6S, HP
2017	8.3 ± 0.5	HP, LP, UF

736
737 [a]standard deviation
738 [b]HP = high prey density (10 rotifer ml^{-1} and 3 natural zooplankton ml^{-1}); LP = low prey density
739 (1.0 natural zooplankton ml^{-1}); UF = unfed; S6F = starved for 6 days then fed; F6S = Fed for 6
740 days then starved

741 Table 2. Additive and variable coefficient generalized additive models formulated to predict
742 Walleye Pollock (*Gadus chalcogrammus*) larvae growth rate. AIC is Akaike Information
743 Criterion.
744

Model Type	Model	AIC	r^2
Model 1 : Additive, standard length used as size covariate	$GR^{a} = a^{b} + s^{c}(t^{d}) + s(sl^{e}) + s(tg2^{f}) + s(ts^{g}) + s(trsg1^{h}) + \varepsilon^{i}$	-1375.68	0.79
Model 2: Additive, product of standard length and body depth at anus used as size covariate	$GR = a + s(t) + s(slbda^{j}) + s(tg2) + s(ts) + s(trsg1) + \varepsilon$	-1247.86	0.68
Model 3: Variable coefficient, cell cycle parameters vary with SL	$GR = a + s(t) + s(sl) + s(sl) \times tg2 + s(sl) \times ts + s(sl) \times trsg1 + \varepsilon$	-1389.55	0.80
Model 4: Variable coefficient, cell cycle parameters vary with temperature	$GR = a + s(sl) + s(t) \times tg2 + s(t) \times ts + \varepsilon$	-1378.39	0.79

745

746 [a]growth rate (growth in length, mm d^{-1})

747 [b]model intercept

748 [c]smooth function

749 [d]rearing temperature

750 [e]standard length

751 [f]arcsin $\sqrt{x}$ transformed fraction of nuclei in the G2-and-M-stage of the cell cycle

752 [g]arcsin $\sqrt{x}$ transformed of nuclei in the S-stage of the cell cycle

753 [h] arcsin $\sqrt{x}$ transformed ratio of the number of cells the S-stage to number of cells in the G1-
754 stage with high nuclear RNA content

755 [i]model error

756 [j]product of standard length and body depth at anus, and is correlated with larval weight (van der
757 Meeren, 1991).

758 Table 3. Rearing temperature, days after first feeding sampled, size range (standard length, mm),
759 and number of larvae (n) used to formulate and validation test the growth models.
760

		Model formulation		Validation testing	
Temperature (°C)	Days sampled	Size range	n	Size range	n
1.6	6, 12, 22	5.33 – 8.30	64	6.42 – 6.90	9
2.8	22	6.54 – 8.84	9		
3.0	6, 12, 25	5.60 – 8.41	72		
3.2	6, 12, 25	5.96 – 9.25	52	6.78 – 8.54	14
6.1	3, 6, 13, 25	5.32 – 11.17	88	7.40 – 8.63	15
8.3	3, 8, 17	5.66 – 8.25	33	7.14 – 8.61	7

761

762 Table 4. Validation testing for growth models 1, 3, and 4 (see Table 2 for description of models).
763 The Pearson correlation coefficient (r) between predicted growth rates and laboratory growth
764 rates, slope of linear regression for laboratory growth rate and predicted growth rate, the
765 percentage of predictions that were correct (i.e., equal to laboratory growth), and percentage of
766 laboratory growth rates within the 95% confidence interval of the predicted growth rates.
767

Model	r	Slope of linear regression	% correct predictions	% of laboratory growth rates within the 95% CI of the predicted growth rates
1	0.83	0.62	16	33
3	0.88	0.58	7	31
4	0.84	0.70	7	27

768

769 Table 5. Laboratory and model predicted growth rate (mm d^{-1}) for each rearing temperature for
770 the independent validation testing data set (see Table 2 for description of models).
771

	Temperature			
	1.6°C, n = 9[b]	3.2°C, n= 14	6.1°C, n= 15	8.3°C, n= 7
Laboratory[a]	0.06[c] ± 0.02	0.08 ± 0.02	0.15 ± 0.03	0.15 ± 0.03
Model 1	0.06 ± 0.01	*0.09 ± 0.02	*0.12 ± 0.02	0.16 ± 0.03
Model 3	0.07 ± 0.01	*0.09 ± 0.02	*0.12 ± 0.02	0.14 ± 0.03
Model 4	0.06 ± 0.01	*0.09 ± 0.02	*0.13 ± 0.02	0.16 ± 0.04
ANOVA[d]	$F_{3,24} = 0.44$, $p = 0.72$	$F_{3,39} = 5.12$, $p = 0.004$	$F_{3,42} = 66.58$, $p < 0.001$	$F_{3,18} = 2.76$, $p = 0.07$

772

773 [a]laboratory growth rate was calculated from size at age (see text)
774 [b]number of larvae tested
775 [c]mean growth rate ± standard deviation
776 [d]repeated measures ANOVA comparing laboratory and model predicted growth rates at each
777 temperature
778 [*]significantly different from laboratory growth rate ($p < 0.05$) as indicated by Tukey Test

779 Table 6. Laboratory growth rate, growth rate derived from otolith microstructure analysis, and
780 growth rate predicted from models 1, 3, and 4 for 6.1° and 8.3°C rearing temperatures of the
781 validation testing data set (19 total larvae, see text for explanation). The Pearson correlation
782 coefficient (r) for predicted growth rates and the distance between the first feeding increment and
783 otolith edge. The percentage of otolith-derived growth rates within the 95% confidence interval
784 of the predicted growth rates.

785

Growth rate type	Growth rate[b]	r	% of otolith-derived growth rates within the 95% CI of the predicted growth rates
Laboratory	0.16 ± 0.03		
Otolith derived[a]	0.17 ± 0.02*		
Model 1	0.13 ± 0.03*	0.91	11
Model 3	0.13 ± 0.02*	0.77	5
Model 4	0.14 ± 0.03	0.81	16

786

787 [a]otolith-derived growth rate was calculated from larval standard length and number of daily
788 increments from first feeding to the otolith edge (see text)

789 [b]mm d^{-1}; mean ± standard deviation

790 *significantly different from laboratory growth rate; repeated measures ANOVA, Tukey test,
791 $p < 0.01$

Table 7. Additive and variable coefficient binomial generalized additive models formulated to predict Walleye Pollock (*Gadus chalcogrammus*) larvae as fast- or slow-growing based on laboratory growth rate of larvae in the high prey density treatment at each temperature. AIC is Akaike Information Criterion.

Classification Model Type	Model	AIC	r^2	% Correct[j]
Model 1: Additive, analogous to growth rate model 1.	$pGR^a = a^b + s^c(t^d) + s(sl^e) + s(tg2^f) + s(ts^g) + s(trsg1^h) + \mathcal{E}^i$	321.61	0.33	69 (31/45)
Model 2: Variable coefficient, cell cycle parameters vary with SL. Similar to growth rate model 3[k].	$pGR = a + s(t) + s(sl) + s(sl) \times tg2 + s(sl) \times ts + \mathcal{E}$	326.87	0.31	71 (32/45)
Model 3: Variable coefficient, cell cycle parameters vary with temperature. Analogous to growth rate model 4.	$pGR = a + s(sl) + s(t) \times tg2 + s(t) \times ts + \mathcal{E}$	325.46	0.31	69 (31/45)

[a]probability that a larva is fast growing

[b]model intercept

[c]smooth function

[d]rearing temperature

[e]standard length

[f]arcsin $\sqrt{x}$ transformed fraction of nuclei in the G2-and-M-stage of the cell cycle

[g]arcsin $\sqrt{x}$ transformed fraction of nuclei in the S-stage of the cell cycle

[h]arcsin $\sqrt{x}$ transformed ratio of the number of cells the S-stage to number of cells in the G1-stage with high nuclear RNA content

[i]model error

[j]percent of larvae correctly classified as fast- or slow-growing, number of correct classifications shown in parenthesis

[k]based on AIC, arcsin $\sqrt{x}$ transformed ratio of the number of cells the S-stage to number of cells in the G1-stage with high nuclear RNA content was not included in the model

812 Table 8. Area sampled, station, water temperature (mean 0-50 m depth; °C), mean size of larvae,
813 mean predicted growth rate, mean otolith-derived growth rate, and mean predicted probability of
814 fast growth for Walleye Pollock (*Gadus chalcogrammus*) larvae collected from the western Gulf
815 of Alaska 18 – 30 May 2013.

816

Area	Station	Date[b]	Temp.	n[c]	SL[d]	Pred. GR[e]	Oto. GR[f]	Prob. fast GR[g]
KI-SI[a]	18	18 May	4.9	1	6.70	0.10	0.20	0.77
KI-SI	78	21 May	4.0	1	9.47	0.14	0.19	0.10
KI-SI	88	22 May	4.6	3	10.36 ± 0.20	0.18 ± 0.01	0.19 ± 0.02	0.99 ± 0.01
KI-SI	89	22 May	4.2	2	8.93 ± 0.83	0.14 ± 0.02	0.18 ± 0.03	0.57 ± 0.16
KI-SI	90	23 May	4.5	3	10.21 ± 0.57	0.17 ± 0.03	0.18 ± 0.01	0.54 ± 0.24
KI-SI	102	23 May	4.5	3	9.90 ± 0.10	0.15 ± 0.003	0.20 ± 0.01	0.71 ± 0.19
KI-SI	103	23 May	4.1	2	10.07 ± 0.66	0.17 ± 0.03	0.19	0.54 ± 0.46
KI-SI	105	23 May	4.3	2	10.40 ± 0.60	0.18 ± 0.04	0.16 ± 0.01	0.79 ± 0.21
Kodiak Is.	161	27 May	5.1	3	12.73 ± 1.33	0.36 ± 0.10	0.17 ± 0.003	1.00
Kodiak Is.	162	27 May	5.1	1	12.10	0.30	0.17	1.00
Kodiak Is.	164	28 May	5.0	4	11.25 ± 0.99	0.26 ± 0.07	0.18 ± 0.01	0.75 ± 0.22
Kodiak Is.	187	29 May	5.5	1	5.91	0.05	-[h]	0.79
Kodiak Is.	191	29 May	6.0	1	12.10	0.32	0.17	1.00
Kodiak Is.	200	30 May	5.9	4	11.00 ± 0.60	0.24 ± 0.04	0.19 ± 0.02	0.93 ± 0.07

817

818 [a]area between Kodiak Island and Shumagin Islands (see Fig. 1)

819 [b]date larvae collected

820 [c]number of larvae analyzed

821 [d]mean standard length ± standard error

[e]model 1 predicted growth rate ± standard error (mm d^{-1}); mean growth rate for all larvae analyzed at a station

[f]otolith-derived growth rate ± standard error (mm d^{-1}) calculated from age (number of increments from first feeding to otolith edge) and standard length

[g]mean probability of fast growth ± standard error; probability ≥ 0.50 indicates fast growth

[h]otoliths from this larva were unreadable due to poor increment definition, so this larva was not used in further analyses

829